Macromolecules
ARTICLE

Macromolecules **2009**, *42*, 6277–6283 **6277**
DOI: 10.1021/ma900895n

Charged Dendrimers on Lipid Bilayer Membranes: Insight through Dissipative Particle Dynamics Simulations

Li-Tang Yan*,† and Xiaobo Yu‡

†*Physikalische Chemie II, Universitat Bayreuth, D-95440 Bayreuth, Germany, and* ‡*Biochemistry Department, NMI Natural and Medical Sciences Institute at the University of Tuebingen, 72770 Reutlingen, Germany*

Received April 24, 2009; Revised Manuscript Received July 2, 2009

ABSTRACT: Understanding the interactions of dendrimers with biological membranes is of fundamental importance in determining their potential biomedical applications like drug delivery vehicles and gene therapeutic agents. Herein we perform systematically mesoscopic simulations to investigate the interactions and binding structures in complexes comprised of charged dendrimers with lipid bilayer membranes. For these purposes, various interaction strengths between the outer-dendrimer hydrophilic component and lipid heads and those between the inner-dendrimer hydrophobic component and lipid tails are used in the simulations. The external force is also induced into the complexes by stretching the membranes to examine the influence of the dendrimer binding on the stabilization of the lipid bilayer membranes. Our simulations demonstrate that the increasing attraction between outer dendrimer and lipid heads leads to wider spread of dendrimer along the membrane surface, while the attraction between the inner dendrimer and lipid tails has a great effect on the insertion of the dendrimer into the bilayer membrane. It is found that the dendrimer can induce a hole in the tense bilayer membrane at earlier time for a stronger attraction between the hydrophobic dendrimer component and lipid tails, which prompts the failure of the membrane affected by the external forces or surroundings. The findings could provide some guidelines for the design of the dendrimers with defined molecular architectures and prompt the understanding for the stabilization of the tense membranes and the potential cytotoxicity of the charged dendrimers in the dendrimer−lipid bilayer membrane complexes.

1. Introduction

The efficient and safe delivery of therapeutic nuclei acids has remained as one of the main problems in gene therapy.[1,2] A way forward is to resort to the use of nanosize delivery vehicles which would effectively compact and protect a guest drug molecule.[3,4] Dendrimers, consisting of regularly branched monomeric building blocks and many surface terminal groups, seem to be good candidates for these purposes due to their unique molecule architectures and related properties.[5−9] In particular, the size, shape, interior density, and surface functionality of dendrimers can be controlled directly, allowing them to serve both as nanodevices and as targeting molecules. For these applications, the dendrimers need to interact with cell membrane. Amphiphilic lipid molecules are essential constituents of cell membranes and the lipid bilayer membranes form the basis of many important cellular organelles, such as the endoplasmic reticulum, the Golgi apparatus, or the vesicular transport system.[10−13] Thereby, a more thorough understanding of the interactions between dendrimers and lipid bilayer membranes will address many relevant issues pertaining to real cells.

Because of the extensive biomedical and technical applications, the complexes comprised charged dendrimers with lipid bilayer membranes have recently attracted considerable attention.[6−9,14−16] Experimentally, by using atomic force microscopy (AFM) and enzyme assays, it has been suggested that the temperature, terminal (charged or uncharged) groups, and size of dendrimers play important roles in the interactions between dendrimers and lipid bilayer membranes.[6−9] On the other hand, tailored computer simulations offer an alternative approach to understand these interactions.[14−18] Only very recently have some involved molecular dynamics (MD) simulations, including atom-detailed and coarse-grained models, emerged.[14−16] For instance, Lee and Larson[14] performed coarse-grained MD simulations to understand the effects of dendrimer size, extent of terminal acetylation, temperature, and salt concentration on dendrimer−lipid bilayer membrane interactions. Their simulations qualitatively reproduce the experimental observations very well.

One of central issues in this field is to determine the effect factors on the final structures of the dendrimer−lipid bilayer membrane complexes. The outer-dendrimer hydrophilic components and inner-dendrimer hydrophobic components may play different roles in the morphology change and binding structures of the dendrimers in the complexes.[15,16] By calculating the enthalpy release in the atomistic MD simulations for the interactions of the charged generation-3 (G3) dendrimer with the lipid bilayer membrane, Kelly et al.[16] show that the stronger binding to fluid lipid membranes is driven by the hydrophobic interaction between the inner dendrimer and lipid tails, which contradicts previous perception that the hydrophilic interaction between outer dendrimer and lipid heads is the dominant factor. However, the atomistic MD simulations are very limited in the range of system size and time scale they can reach. Moreover, a direct view of the morphology change and binding structures of the dendrimers in the complexes is particularly necessary to examine the roles of these various interactions.

Herein we use a mesoscopic simulation technique, dissipative particle dynamics (DPD), to consider this important topic.[19,20] DPD offers an approach that can be used for modeling physical phenomena occurring at larger time and spatial scales than some

*To whom correspondence should be addressed.

Published on Web 07/14/2009

other classic methods as it utilizes a momentum-conserving thermostat and soft repulsive interactions between the beads representing clusters of molecules.[21−25] Thus, by employing this method, we can study the complexes between charged generation-5 (G5) dendrimers and 18 nm × 18 nm planar lipid bilayer membranes over 15 μs. Although our simulations focus on the interactions between the amphiphilic moieties in the dendimers and those in the lipid molecular, the long-range electrostatic interactions and explicit counterions are also included in the simulations because the counterion condensation and the interactions between the counterions and the charged groups may affect the complex structure to a certain extent. Furthermore, the external force is also induced into the complexes by stretching the membrane in order to examine the influence of the dendrimer insertion on the stabilization of the lipid bilayer membranes and the potential cytotoxicity of the charged dendrimers in the dendrimer−bilayer membrane complexes.

2. Method and Model Details

In DPD, a numbers of atoms are coarse-grained into a single DPD bead according to their chemical identity and their environment.[19,20] The beads interact with each other by pairwise additive forces that locally conserve momentum and lead to the correct hydrodynamics. In the present simulations, a bead i at position $\mathbf{r}_i$ surrounded by beads $j \neq i$ at $\mathbf{r}_j$ (distance vector $\mathbf{r}_{ij}=\mathbf{r}_i-\mathbf{r}_j$ and unit vector $e_{ij} = \mathbf{r}_{ij}/r_{ij}$ with $r_{ij} = |\mathbf{r}_{ij}|$) experiences a force with the components of conservative interaction force F^C, dissipative force F^D, random force F^R, bond force F^S (including harmonic bond force and bond angle force), and the electrostatic force F^E, i.e., $f_i=\sum_{j\neq i}(F^C_{ij} + F^D_{ij} + F^R_{ij} + F^S_{ij} + F^E_{ij})$, where the sum runs over all beads j.

The conservative force is soft repulsion term that acts along the lines of the centers and is given by $F^C_{ij}=\alpha_{ij}\omega^C(r_{ij})e_{ij}$, where α_{ij} is the maximum repulsion between beads i and j which can be mapped onto the Flory−Huggins χ_{ij} parameter by a simple linear equation.[20] The detailed interaction parameters of χ_{ij} in the present simulations can be found in Table S1 of the Supporting Information. In the simulations, we change the interaction parameters between the hydrophilic dendrimer component and lipid heads, χ_{HC}, and the interaction parameters between the hydrophobic dendrimer component and lipid tails, χ_{TU}, to concern these interactions on the binding structures in complexes comprised of charged dendrimers with lipid bilayer membranes. The increase of χ_{HC} and χ_{TU} corresponds to the stronger bead repulsion while the decrease of these Flory−Huggins parameters leads to the stronger bead attraction. In order to ensure the conservative force soft and repulsive, the weight function $\omega^C(r_{ij})$ is chosen as $\omega^C(r_{ij})=1-r_{ij}/r_c$ for $r_{ij} < r_c$ and $\omega^C(r_{ij})=0$ for $r_{ij} \geq r_c$, where r_c is the truncate distance.

The velocity-dependent dissipative force F^D_{ij} provides a viscous drag to the beads, whereas the random term F^R_{ij} counteracts this cooling by applying random kicks to the beads that tend to increase the relative velocities of the adjacent pairs. They are given by $F^R_{ij}=\sigma\omega(r_{ij})\xi_{ij}\Delta t^{-1/2}e_{ij}$ and the dissipative force $F^D_{ij}=-1/2\sigma^2\omega(r_{ij})(v_{ij}\ e_{ij})e_{ij}$, where $v_{ij} = v_i - v_j$ and v_i denotes the velocity of bead i. ξ_{ij} is a random number which has zero mean and unit variance.[20] The noise amplitude, σ, is fixed at $\sigma=3$ in the present simulations.

Hookean springs with the potential $U_s(i, i+1) = (1/2)k_s(|r_{i,i+1}| - l_0)^2$ is used to construct dendrimers and lipids, where i, $i+1$ represent connecting beads in the molecules.[22,23] The spring constant, $k_s=64$, and unstretched length, $l_0=0.5r_c$, are chosen so as to fix the average bond length to a desired value. A three-body potential acting between adjacent bead triples in each tail of lipids and the branches of dendrimer, $U_a(i-1, i, i+1)=k_a[1-\cos(\phi-\phi_0)]$ is selected to model the chain stiffness, where the angle ϕ is defined by the scalar product of the two bonds connecting beads $i-1$, i, and i, $i+1$.[22,23] The bending constant $k_a=20$ is used for both lipid and dendrimer. The preferred angle, ϕ_0, is specified 0° and 120° for lipid tails and dendrimer branches, respectively. The bond force F^S (including harmonic bond force and bond angle force) is then calculated based on the differential forms of these potentials.

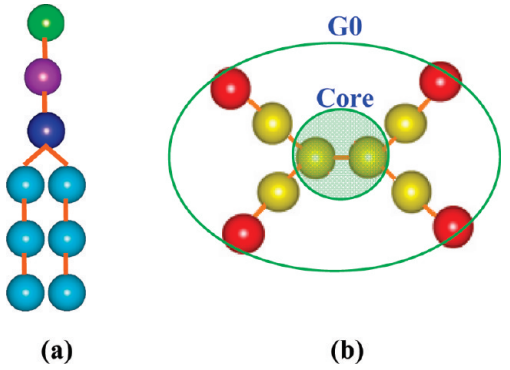

Figure 1. Schematic diagrams showing the DPD models for the simulated molecules of phospholipid (a) and charged dendrimer (b). Model b is only a 0-generation (G0) dendrimer indicating the constructing route for the dendrimers with more generation. In the phospholipid model (a), the colors of the beads stand for hydrophilic headgroup with charge +1 (green), hydrophilic headgroup with charge −1 (pink), headgroup without charge (blue), and hydrophobic tail group (cyan). In model b, i.e., the charged dendrimer, the yellow beads constitute the hydrophobic moiety of the dendrimer, while the red beads are hydrophilic and each red one carries a charge of +1.

The electrostatic force F^E_i is analyzed based on a modification particle−particle−particle−mesh (P3M) algorithm due to Groot,[26] in which the electrostatic field is solved by smearing the charges over lattice grid whose size is determined by a balance between the fast implementation and the correct representation of the electrostatic field. The detailed form of the force F^E_i can be found in ref 26 and our previous works.[27] In the present simulations the grid size is set to r_c. The truncate distance for the electrostatic interaction is selected as $1.6r_c$. The coupling constant Γ is set to 13.87, which corresponds to the Bjerrum length of water at room temperature (about $1.1r_c$).[26]

Similar to MD simulations, DPD captures the time evolution of many-body system through the numerical integration of Newton's equation of motion. Here we use a modified velocity-Verlet algorithm due to Groot and Warren to solve the motion equation.[20] In the simulations, the radius of interaction, the bead mass, and the temperature are set as the unit, i.e., $r_c=m=k_BT=1$. A characteristic time scale is then defined as $\tau = (mr_c^2/k_BT)^{1/2}$. Our simulation box is $(26r_c)^3$ in size and with periodic boundary condition in all directions. The simulation results by using a larger simulation box with $(36r_c)^3$ demonstrate that the simulation box used here is large enough to avoid the finite size effects. Considering the calculation economy, we select the simulation box with $(26r_c)^3$ in the present simulations. A bead number density of $3/r_c^3$ is selected. The time step of $\Delta t=0.02\tau$ is selected, ensuring the accurate temperature control of the simulation system.[28,29]

Full technical details on the models of lipid and the charged dendrimer can be found in Figure 1. Briefly, each amphiphilic lipid consists of a headgroup and two tails. The headgroup contains three connected hydrophilic beads, and the top two of them carry the charges of +1 and −1. Each tail includes three connected hydrophobic beads. The model of charged dendrimer is mapped from the polyamidoamine (PAMAM)-like dendrimer.[6−8] Only the terminal beads of the dendrimer model are hydrophilic and carry the charge of +1. The other moiety of

the dendrimer is uncharged and hydrophobic. Note that here we do not attempt to concern specific dendrimers and lipid molecules and their interactions. Solvent particles are represented by a single bead.

The typical area per lipid in a tensionless dipalmitoylphosphatidylcholine (DPPC) membrane is about 0.64 nm^2.[21] We use this value to estimate the physical length of our simulations and find that r_c is about 0.7 nm. Thereby, the area of the tensionless membrane in our simulation is 18 nm × 18 nm. The time unit τ is related to the physical time by comparing the in-plane diffusion coefficient of lipids. A typical experimental result of this coefficient is 5 $\mu m^2/s$.[24] Equating this value to the simulation result yields τ = 7.7 ns, and thus the total physical time of each calculation is about 15 μs (10^5 time steps).

3. Results and Discussion

The DPD method has been applied successfully to study the conformational behaviors and the interactions in the charged macromolecules, e.g., cylindrical polyelectrolyte brush.[27] However, the charged dendrimers have yet not been concerned by this method. To examine its efficiency in the investigation of the charged dendrimers, we simulate the charged G3, G5, and generation-7 (G7) dendrimers first. Figure 2 shows the structures and sizes of these dendrimers at the equilibrium state. After comparing with the corresponding experiments or other simulations, we find that our simulation can reproduce the structures and the sizes of the charged dendrimers with various generations very well.[14,30]

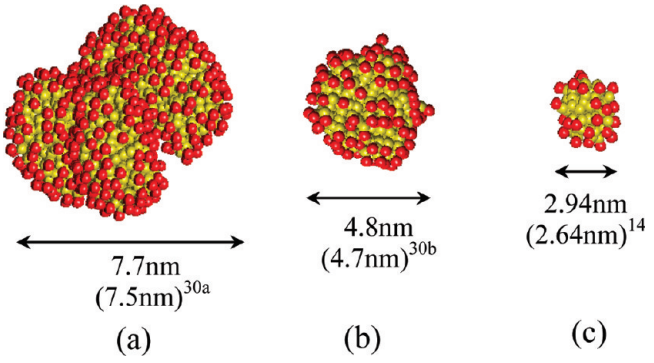

Figure 2. Snapshots of typical equilibrium configurations of G7 (a), G5 (b), and G3 (c) dendrimers. The radius of gyration of each dendrimer and its corresponding value in the literatures (in parentheses) are marked at bottom. The yellow beads constitute the hydrophobic moiety in the dendrimer, while the red beads are hydrophilic and each red bead carries a charge of +1. The counterions are not shown for clarity.

At the beginning of our simulations, a stable, tensionless square bilayer membrane, that is in the fluid state and consists of 1054 lipids, is also obtained. The area per lipid, A_l, of this membrane is about $1.28r_c^2$. A charged G5 dendrimer is used in the simulations, and its equilibrated radius of gyration is about 2.4 nm, comparable to the experimental result of PAMAM dendrimer.[30] An equilibrium dendrimer then be added to the lipid bilayer membrane system in which the lowest beads of the dendrimer are adjacent to the top surface of the membrane. To preserve charge neutrality, the randomly selected solvent beads in the membrane system are changed into the counterions of a charge of −1. Figure 3a shows the initial arrangement of the lipid bilayer membrane and the charged G5 dendrimer. The lateral density profiles of the hydrophobic and hydrophilic beads of the membrane and the dendrimer, together with the water beads, are shown in Figure 3b. It can be found that the hydrophilic lipid heads form the two surfaces of the bilayer membrane with the hydrophobic lipid tails confined between them. The solvent is excluded from the hydrophobic region of the membrane due to the strong solvent−lipid tail repulsion.

3.1. Effects of the Interaction Parameters on the Morphology and Binding of the Dendrimers. It has been suggested through the energy calculation in MD simulations that the outer-dendrimer hydrophilic components and inner-dendrimer hydrophobic components play different roles in the morphology change and binding structures of the dendrimers in the dendrimer−bilayer membrane complexes.[15,16] In this section we gain insight into this important topic by changing the interaction parameters between the hydrophilic dendrimer component and lipid heads, χ_{HC}, and the interaction parameters between the hydrophobic dendrimer component and lipid tails, χ_{TU}. The increase of χ_{HC} and χ_{TU} corresponds to the stronger bead repulsion while the decrease of these Flory−Huggins parameters leads to the stronger bead attraction.

Figure 4 shows the snapshots of the complexes comprised the charged G5 dendrimer with the lipid bilayer membrane at χ_{TU} = 0.92 and different χ_{HC}. The dendrimer spreads along the surface of the bilayer membrane at χ_{HC} = −6.12 because of the strong attraction between the outer-dendrimer hydrophilic component and the lipid heads. With the increasing χ_{HC}, the dendrimer collapses and its spreading scale becomes narrow. However, one can note from the cross-sectional views that, with the increasing χ_{HC}, the binding structure

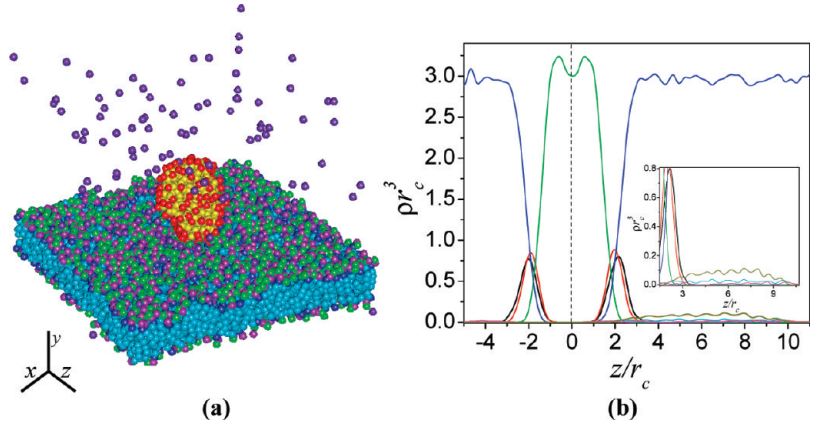

Figure 3. (a) Arrangement of the lipid bilayer membrane and the charged G5 dendrimer at the initial time (0 μs). The density profiles for different types of beads in (a) are plotted in (b) and its inset. In (a), the color code is the same as that in Figure 1 except that the violet beads represent the counterions of a charge of −1. Solvent is not shown for clarity. In (b), the profile color scheme: head beads with positive charge (black), head beads with negative charge (red), tail beads (green), water beads (blue), dendrimer beads with positive charge (cyan), uncharged dendrimer beads (dark green), and counterions (pink).

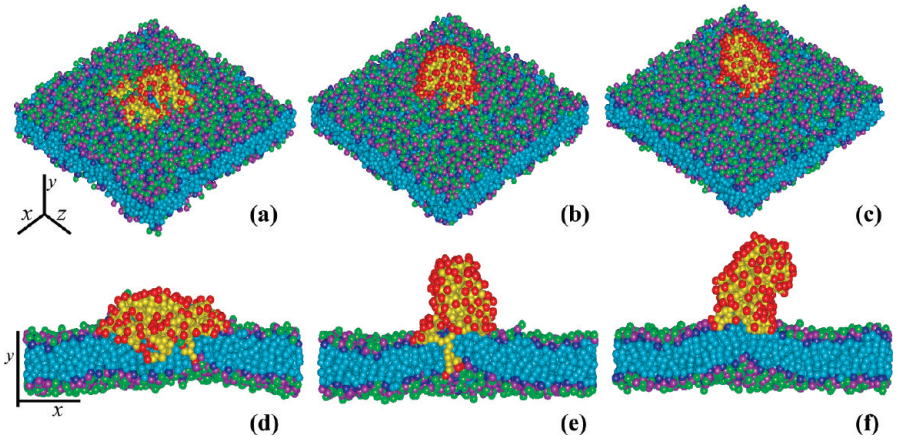

Figure 4. Complexes between the charged G5 dendrimer and the lipid bilayer membrane at different interaction parameters between lipid heads and outer-dendrimer hydrophilic component, χ_{HC}. Panels (d), (e), and (f) are the cross-sectional views of panels (a), (b), and (c) respectively. χ_{HC} = −6.12 (a, d), −3.06 (b, e), and −0.92 (c, f). The interaction parameter between lipid tails and inner hydrophobic dendrimer χ_{TU} is fixed at 0.92. The time for each simulation snapshot is 15 μs. The color code is the same as that in Figure 1. Solvent and counterions are not shown for clarity.

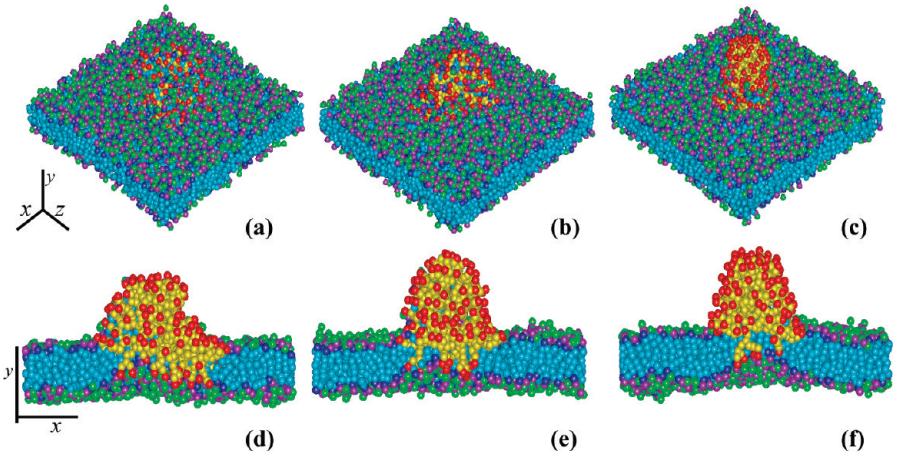

Figure 5. Complexes between the charged G5 dendrimer and the lipid bilayer membrane at various interaction parameters between the lipid tails and the inner-dendrimer hydrophobic component, χ_{TU}. Panels (d), (e), and (f) are the cross-sectional views of the panels (a), (b), and (c) respectively. χ_{TU} = −4.59 (a, d), −3.06 (b, e), and −0.92 (c, f). The interaction parameter between the lipid heads and outer hydrophilic dendrimer χ_{HC} is fixed at −3.06. The time for each simulation snapshot is 15 μs. The color code is the same as that in Figure 1. Solvent and counterions are not shown for clarity.

of the dendrimer has very small change, and only a few dendrimer beads can insert into the bilayer membrane even at χ_{HC} = −6.12. Clearly, the change of the interaction between the hydrophilic dendrimer component and lipid heads has a very light effect on the insertion of the dendrimer whereas it can influence the dendrimer morphology to a great extent.

The snapshots of the complexes comprised the charged G5 dendrimer with the lipid bilayer membrane at χ_{HC} = −3.06 and various χ_{TU} are illustrated in Figure 5. For a strong attraction between the inner-dendrimer hydrophobic component and the lipid tails, large numbers of lipids are pulled away from the original membrane and migrate onto the dendrimer (Figure 5a), which has also been observed in the corresponding experiments.[7,8] Simultaneously, one can find that many dendrimer beads insert into the membrane. With the increasing, both the lipids migrating onto the dendrimer and the dendrimer beads inserting into the membrane decrease obviously (Figure 5b,c). We thus conclude that the hydrophobic interaction between the inner-dendrimer component and the lipid tails has a great effect on the binding structure of the dendrimer.

To test the changes of the dendrimer morphology quantitively, we calculate the radius of gyration (R_g) and the asphericity (A_s). The gyration radius of the dendrimer is defined as

$$R_g^2 = \langle \frac{1}{N} \sum_{i=1}^{N} (\mathbf{r}_i - \mathbf{r}_{CM})^2 \rangle \quad (1)$$

where the summation runs over the N positions $\mathbf{r}_i$ of every bead of the dendrimer and $\mathbf{r}_{CM}$ is the center of mass of the dendrimer. The asphericity of the dendrimer is defined as[31,32]

$$A_s = 1 - 3\langle I_2 \rangle / \langle I_1^2 \rangle \quad (2)$$

where I_1 and I_2 are the first two invariants

$$I_1 = \lambda_1 + \lambda_2 + \lambda_3 \quad (3)$$

$$I_2 = \lambda_1\lambda_2 + \lambda_2\lambda_3 + \lambda_1\lambda_3 \quad (4)$$

and λ_1, λ_2, and λ_3 are the eigenvalues of the gyration tensor

$$G_{uv} = \frac{1}{N} \sum_{i}^{N} (\mathbf{r}_{ui} - R_{gu})(\mathbf{r}_{vi} - R_{gv}) \quad (5)$$

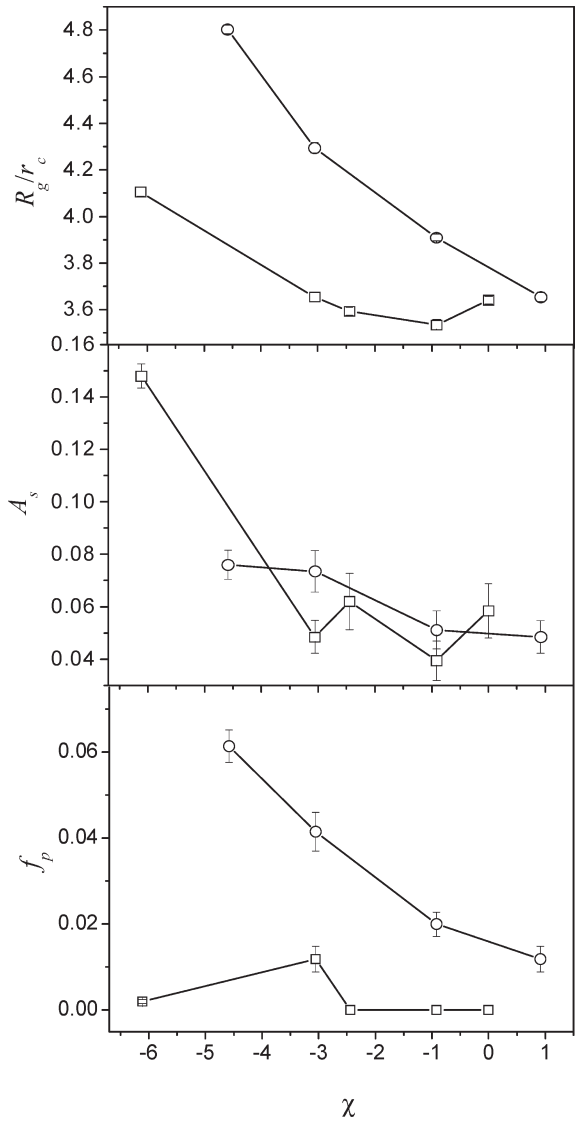

Figure 6. Radius of gyration (R_g), asphericity (A_s), and permeable fraction (f_p) of the charged G5 dendrimer as functions of the bead interaction χ. Squares: interaction parameters between the lipid heads and the outer-dendrimer hydrophilic component, χ_{HC}, where $\chi_{TU} = 0.92$. Circles: interaction parameters between the lipid tails and the inner-dendrimer hydrophobic component, χ_{TU}, where $\chi_{HC} = -3.06$. The calculating time for each point is 15 μs.

where u and $v = x, y, z$. Corresponding to the form of the dendrimer, the asphericity parameter can take values ranging from zero (sphere) to one (line). To further analyze the binding structure of the dendrimer, we quantify the penetrability of the dendrimer by the fraction of permeable dendrimer beads (f_p). Here the permeable dendrimer beads are defined as the dendrimer beads beyond the middle or reach the other side of the bilayer membrane during the simulation period (15 μs).

In Figure 6, we present the R_g, A_s, and f_p of the dendrimer as functions of the bead interaction parameter. As expected, the size of the dendrimer will decrease when we strengthen the bead repulsion interaction; i.e., χ (including χ_{HC} and χ_{TU}) becomes larger. For χ_{TU}, the decrease of the dendrimer size is due to the fact that fewer lipids can be pulled out from the membrane and can migrate onto the dendrimer in the presence of a stronger repulsion between the inner-dendrimer hydrophobic component and the lipid tails. For χ_{HC}, the narrower spread of the dendrimer occurs for a stronger repulsion between the outer-dendrimer hydrophilic component and the lipid heads which leads to the collapse of the dendrimer. It can be seen from Figure 6 that, when the outer-dendrimer hydrophilic component has a strong attraction to the lipid head, A_s is very large due to the wider spread of the dendrimer, corresponding to Figure 3a. Accompanying with the collapse of the dendrimer, the asphericity A_s becomes small, demonstrating that the dendrimer is prone to exhibit a spherical form for a larger χ_{HC} or χ_{TU}. Figure 6 also shows that the permeable fraction of the dendrimer f_p remains almost unchangeable with the increasing χ_{HC} while it can be influenced by the variation of χ_{TU} to a great extent. This reveals that the attraction between the inner-dendrimer hydrophobic component and lipid tails has a dominant effect on the insertion of the dendrimer into the bilayer membrane.

One of the major implications for this finding is that the morphology and binding structures of the dendrimers in the dendrimer−bilayer membrane complexes can be tuned by controlling the hydrophilic interaction between outer dendrimer and lipid heads or the hydrophobic interaction between inner dendrimer and lipid tails. The results obtained from these mesoscopic simulations could provide some guidelines for the design of the dendrimers with defined molecular architectures and functions.

3.2. Dendrimer-Induced Hole in the Tense Lipid Bilayer Membrane. So far, only the tensionless membrane has been concerned in the studies for the dendrimer−bilayer membrane complexes. However, in many cases, the surface tension of the membrane can be altered by either application of an external force or varying the surroundings like temperature, pH, or salt concentration (or osmotic pressure).[33,34] Here we induce the external force into the complexes by stretching the membrane. Consequently, the influence of the dendrimer insertion on the stabilization of the tense lipid bilayer membranes and the potential cytotoxicity of the charged dendrimers can be explored.

We stretch the bilayer membrane by changing the lateral dimensions of the simulation box and simultaneously modify the height of the box to keep the volume of the system constant, i.e., $(x, y, z) \rightarrow (\delta x, \delta y, z/\delta^2)$, where x, y, and z are the coordinates of the box. The system is left to equilibrate over 154 ns, after which time the box is stretched by using a factor $\delta = 1.02$. Simultaneously, the surface tension and the area per lipid, A_l, are recorded. In our simulations, the surface tension is determined by using the formula[35]

$$\gamma_s = \langle (L_y/2)[(P_{yy} - (P_{xx} + P_{zz})/2)] \rangle \quad (6)$$

where P_{ij} is the ij component of the pressure tension and L_y is the box length along the y direction. The last point of the surface tension at each stretching is used as the surface tension at the corresponding area per lipid A_l.

Video S1 of the Supporting Information shows a detailed evolution of a charged G5 dendrimer−bilayer membrane complex with $\chi_{HC} = -3.06$ and $\chi_{TU} = -4.59$ when the external force is applied to it. One can find that the holes will occur in the membrane, and ultimately, the membrane ruptures and fails completely. The video monitors the actual creation and expansion of these holes. Interestingly, besides the holes in the bulk membrane, a hole appears along the rim of the dendrimer. To analyze the hole formation in the tense membrane in more detail, we vary the interaction parameter between the inner-dendrimer hydrophobic component and the lipid tails, χ_{TU}. It can be observed that the hole along the rim of the dendrimer appears in all complexes with various χ_{TU}, indicating that the hole is induced by the charged dendrimer.

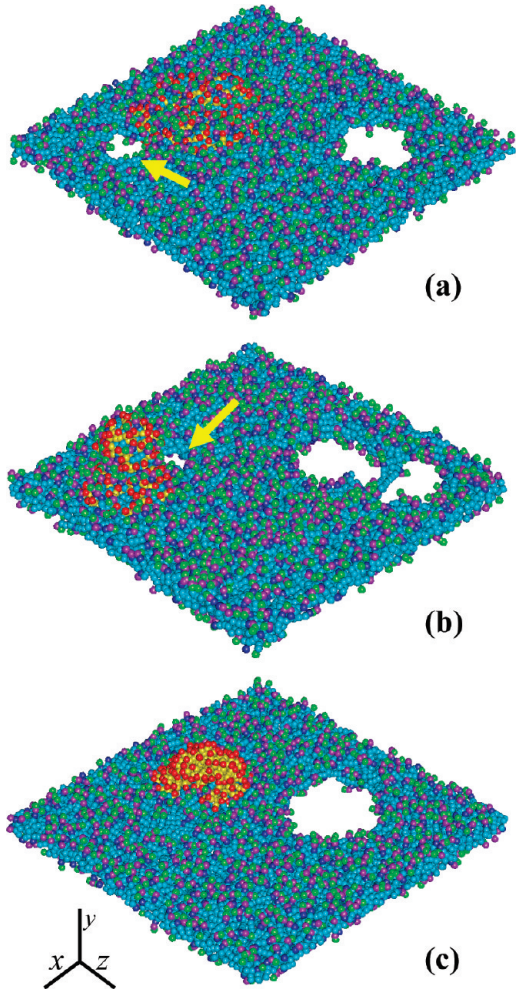

Figure 7. Initial positions of the holes in the tense bilayer membrane-charged G5 dendrimer complexes with $\chi_{TU} = -4.59$ (a), -3.06 (b), and 0.92 (c). The stretching time for each simulation snapshot is 2.77 (a), 2.93 (b), and 2.93 μs (c). The arrows in (a) and (b) show the incipient holes near the dendrimer. The color code is the same as that in Figure 1. Solvent and counterions are not shown for clarity.

Figure 7 presents the snapshots with different χ_{TU} illustrating the initial positions of the holes in the tense dendrimer−membrane complexes. Clearly, the dendrimer can induce a hole in the tense bilayer membrane at earlier time for a stronger attraction between the hydrophobic dendrimer component and lipid tails, which can also be found in the inset of Figure 8. The previous simulations for single tense membrane show that the pore nucleation, which finally leads to the hole with large size, in a bilayer membrane is an activated process because there is an energy barrier which ensures the integrity of the membrane.[36] Our simulations indicate that the presence of the charged dendrimer is helpful to invoke this activity and the stronger attraction between the hydrophobic dendrimer component and lipid tails can overcome the energy barrier more easily.

Figure 8 shows the surfaces tension as functions of A_l at various χ_{TU}. It can be seen that the membranes rupture at almost the same A_l demonstrating that the hydrophobic interaction between the inner dendrimer and lipid tails has light effect on the tolerances (maximum stretch) of the membranes. Note that in Video S1 and Figure 7 the rupture of all membranes begin with the formation of the hole in the bulk membrane which occurs at almost the same time for these three χ_{TU}. However, the hole along the rim of the

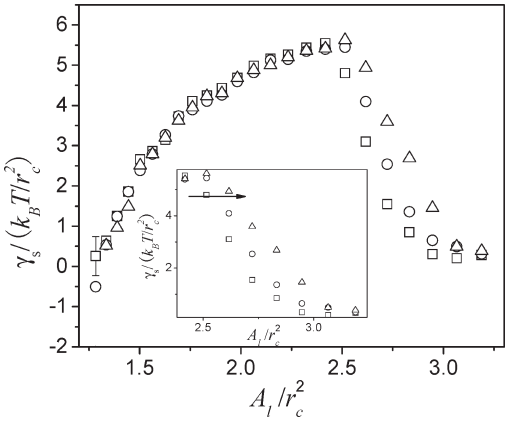

Figure 8. Surface tension as functions of the area per lipid for the complexes comprised of the bilayer membrane with the charged G5 dendrimer at $\chi_{HC} = -3.06$ and various χ_{TU}. $\chi_{TU} = -4.59$ (squares), -3.06 (circles), and 0.92 (triangles). All error bars are similar to the one shown. The inset shows these plots after membrane rupture.

dendrimer appears earlier for a larger χ_{TU}. (Here the A_l can also reflect the total stretching time for the membranes because, as stated above, the stretched factor and equilibrium time are the same at each stretching.) Consequently, a faster decrease of the surface tension appears in the complexes with larger χ_{TU} after the crossovers in the surface tension curves. The trends predicted here imply that a stronger attraction between the inner-dendrimer hydrophobic component and lipid tails can prompt the failure of the membrane affected by the external forces or surroundings.

4. Conclusions

We have performed a systematic DPD simulation study for the interactions and binding structures in complexes comprised of charged dendrimers with lipid bilayer membranes. For these purposes, we varied the interaction strengths between the outer-dendrimer hydrophilic component and lipid heads and those between the inner-dendrimer hydrophobic component and lipid tails. The external force was also induced into the complexes by stretching the membranes. Our simulations demonstrate that the increasing attraction between outer dendrimer and lipid heads leads to wider spread of dendrimer along the membrane surface, while the attraction between the inner dendrimer and lipid tails has a great effect on the insertion of the dendrimer into the bilayer membrane. It was found that the dendrimer can induce a hole in the tense bilayer membrane at earlier time for a stronger attraction between the hydrophobic dendrimer component and lipid tails, which prompts the failure of the membrane affected by the external forces or surroundings. These findings highlight the fact that the morphology and binding structures of the dendrimer in the dendrimer−bilayer membrane complexes can be tuned by controlling the hydrophilic interaction between outer dendrimer and lipid heads and the hydrophobic interaction between the inner dendrimer and lipid tails. The demonstrated simulation results could provide some guidelines for the design of the dendrimers with defined molecular architectures and prompt the understanding for the stabilization of the tense membranes and the potential cytotoxicity of the charged dendrimers in the dendrimer−bilayer membrane complexes.

Acknowledgment. We thank Dr. Markus Muller and Dr. Youyong Xu for their help on the calculation and valuable discussion. L.-T.Y. acknowledges the hospitality of Prof. Alexander Böker

and Prof. Andreas Fery at the University of Bayreuth. The financial support from Alexander von Humboldt Foundation is highly appreciated.

Supporting Information Available: Repulsion parameters of the conservative force used in the simulations and a video about a detailed evolution of a dendrimer−lipid bilayer membrane complex undergoing the external force. This material is available free of charge via the Internet at http://pubs.acs.org.

References and Notes

(1) Pack, D. W.; Hoffman, A. S.; Pun, S.; Stayton, P. S. *Nat. Rev. Drug Discovery* **2005**, *4*, 581.
(2) Manunta, M.; Tan, P. H.; Sagoo, P.; Kashefi, K.; George, A. J. T. *Nucleic Acids Res.* **2004**, *32*, 2730.
(3) Qiao, R.; Roberts, A. P.; Mount, A. S.; Klaine, S. J.; Ke, P. C. *Nano Lett.* **2007**, *7*, 614.
(4) Chithrani, B. D.; Ghazani, A. A.; Chan, W. C. W. *Nano Lett.* **2006**, *6*, 662.
(5) Tomalia, D. A. *Prog. Polym. Sci.* **2005**, *30*, 294.
(6) Leroueil, P. R.; Hong, S. Y.; Mecke, A.; Baker, J. R.; Orr, B. G.; Banaszak Holl, M. M. *Acc. Chem. Res.* **2007**, *40*, 335.
(7) Hong, S. P.; Bielinska, A. U.; Mecke, A.; Keszler, B.; Beals, J. L.; Shi, X. Y.; Balogh, L.; Orr, B. G.; Baker, J. R.; Banaszak Holl, M. M. *Bioconjugate Chem.* **2004**, *15*, 774.
(8) Mecke, A.; Majoros, I. J.; Patri, A. K.; Baker, J. R.; Banaszak Holl, M. M. *Langmuir* **2005**, *21*, 10348.
(9) Landmark, K. J.; DiMaggio, S.; Ward, J.; Kelly, C. V.; Vogt, S.; Hong, S.; Kotlyar, A.; Penner-Hahn, J. E.; Baker, J. R.; Banaszak Holl, M. M.; Orr, B. G. *ACS Nano* **2008**, *2*, 773.
(10) Kuokowska-Latallo, J. F.; Bielinska, A. U.; Johnson, J.; Spindler, R.; Tomalia, D. A.; Baker, J. R. *Proc. Natl. Acad. Sci. U.S.A.* **2006**, *93*, 4897.
(11) McMahon, H. T.; Gallop, J. L. *Nature* (*London*) **2005**, *438*, 590.
(12) Tieleman, D. P.; Leontiadou, H.; Mark, A. E.; Marrink, S. J. *J. Am. Chem. Soc.* **2003**, *125*, 6382.
(13) Reynwar, B. J.; Iiiya, G.; Harmandaris, V. A.; Muller, M. M.; Kremer, K.; Deserno, M. *Nature* (*London*) **2007**, *447*, 461.
(14) Lee, H.; Larson, R. G. *J. Phys. Chem. B* **2006**, *110*, 18204.
(15) Kelly, C. V.; Leroueil, P. R.; Nett, E. K.; Wereszczynski, J. M.; Baker, J. R.; Orr, B. G.; Banaszak Holl, M. M.; Andricioaei, I. *J. Phys. Chem. B* **2008**, *112*, 9337.
(16) Kelly, C. V.; Leroueil, P. R.; Orr, B. G.; Banaszak Holl, M. M.; Andricioaei, I. *J. Phys. Chem. B* **2008**, *112*, 9346.
(17) Yan, L.-T.; Yu, X. *ACS Nano*, doi: 10.1021/nn9004236.
(18) Ginzburg, V. V.; Balijepalli, S. *Nano Lett.* **2007**, *7*, 3716.
(19) Hoogerbrugge, P. J.; Koelman, J. *Europhys. Lett.* **1992**, *19*, 155.
(20) Groot, R. D.; Warren, P. B. *J. Chem. Phys.* **1997**, *107*, 4423.
(21) Smith, K. A.; Jasnow, D.; Balazs, A. C. *J. Chem. Phys.* **2007**, *127*, 084703.
(22) Alexeev, A.; Uspal, W. E.; Balazs, A. C. *ACS Nano* **2008**, *2*, 1117.
(23) Shillcock, J. C.; Lipowsky, R. *J. Chem. Phys.* **2002**, *117*, 5048.
(24) Shillcock, J. C.; Lipowsky, R. *Nat. Mater.* **2005**, *4*, 225.
(25) Laradji, M.; Sunil Kumar, P. B. *Phys. Rev. Lett.* **2004**, *93*, 198105.
(26) Groot, R. D. *J. Chem. Phys.* **2003**, *115*, 11265.
(27) (a) Yan, L.-T.; Xu, Y.; Ballauff, M.; Muller, A. H. E.; Böker, A. *J. Phys. Chem. B* **2009**, *113*, 5104. (b) Yan, L.-T.; Zhang, X. *Soft Matter* **2009**, *5*, 2101.
(28) Vattulainen, I.; Karttunen, M.; Besold, G.; Polson, J. M. *J. Chem. Phys.* **2002**, *116*, 3967.
(29) Allen, M. P. *J. Phys. Chem. B* **2006**, *110*, 3823.
(30) (a) Maiti, P. K.; Messina, R. *Macromolecules* **2008**, *41*, 5002. (b) Choi, Y.; Mecke, A.; Orr, B. G.; Banaszak Holl, M. M.; Baker, J. R. *Nano Lett.* **2004**, *4*, 391.
(31) Rudnick, J.; Gaspari, G. *J. Phys. A* **1986**, *19*, L191.
(32) Aronovitz, J.; Nelson, D. *J. Phys.* (*Paris*) **1986**, *47*, 1445.
(33) Petelska, A. D.; Figaszewski, Z. A. *Biophys. J.* **2000**, *78*, 812.
(34) Idiart, M. A.; Levin, Y. *Phys. Rev. E* **2004**, *69*, 061922.
(35) Rao, M.; Levesque, D. *J. Chem. Phys.* **1976**, *65*, 3233.
(36) Wang, Z. J.; Frenkel, D. *J. Chem. Phys.* **2005**, *123*, 154701.